J Mater Sci (2024) 59:5698–5716

Processing Bulk Nanostructured Materials

Multi-scale investigation of microstructure and texture evolution during equal channel angular pressing of silver

Satyam Suwas[1,2,*], Werner Skrotzki[2,*], Nils Scheerbaum[2], Thierry Grosdidier[3,4], Jean-Jacques Fundenberger[3,4], Laszlo S. Tóth[3,4], and Heinz-Günter Brokmeier[5,6]

[1] *Department of Materials Engineering, Indian Institute of Science, Bangalore 560012, India*
[2] *Institute of Solid State and Materials Physics, Dresden University of Technology, 01062 Dresden, Germany*
[3] *Laboratory of Excellence on Design of Alloy Metals for Low Mass Structures (DAMAS), Université de Lorraine, 57045 Metz, France*
[4] *Laboratoire d'Étude des Microstructures et de Mécanique des Matériaux (LEM3), CNRS UMR 7239, Université de Lorraine, 57045 Metz, France*
[5] *Institute of Materials Science and Engineering, Clausthal University of Technology, 38678 Clausthal-Zellerfeld, Germany*
[6] *Helmholtz-Zentrum Hereon GmbH, 21502 Geesthacht, Germany*

Received: 11 October 2023
Accepted: 10 December 2023
Published online: 18 January 2024

ABSTRACT

A multi-scale investigation was carried out on pure silver subjected to equal channel angular pressing up to 3 passes. Microstructure and texture were examined using scanning and transmission electron microscopy as well as diffraction of neutron and high-energy synchrotron radiation. The evolution of the deformation substructure in the material is in accordance with its low stacking fault energy followed by restoration mechanisms leading to overall microstructural refinement. The restoration mechanism sets in as early as after 3 passes. Twinning involved in the deformation process supports grain refinement through mechanisms of dynamic recrystallization involving strain-induced boundary migration contributing to a steady-state grain size. The global texture, as measured by neutron diffraction, forms through a twin-assisted deformation mechanism. The texture is found heterogeneous through thickness.

Handling Editor: Megumi Kawasaki.

Address correspondence to E-mail: satyamsuwas@materials.iisc.ernet.in; werner.skrotzki@tu-dresden.de

https://doi.org/10.1007/s10853-023-09266-w

GRAPHICAL ABSTRACT

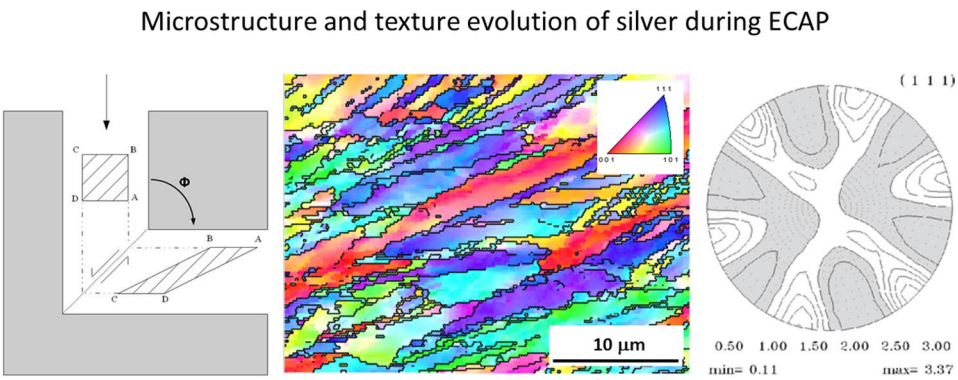

Introduction

Equal channel angular pressing (ECAP) is a severe plastic deformation (SPD) technique for obtaining ultra-fine grain size in bulk materials [1–3]. In ECAP, a billet is made to pass through a die containing two channels intersecting at an angle (generally 90° or 120°) with equal area of cross-section. During ECAP the billet undergoes severe plastic deformation (mainly by shear along the intersection plane of the channels) but retains its original cross-sectional geometry that makes it possible to repeat the process a number of times, each one refining the grain size. Between subsequent passes, it is also possible to rotate the billet around its longitudinal and transverse axis, creating different ECAP routes [4, 5]. All the routes, including route *A*, invariably bring a change in strain path which significantly affects the grain refinement and grain shape due to the high accumulative strain and the interaction of the shearing plane with crystal structure and deformation texture. High strains introduce large misorientations within the subdivided grains; consequently, multi-pass ECAP leads to ultra-fine grain sizes down to the sub-micron level.

It is well known that the deformation mechanism of face-centred cubic (FCC) metals is influenced by the stacking fault energy (SFE), which in turn gives an idea whether the deformation is mediated by slip alone or by slip plus twinning. This difference has been well known to bring significant differences in texture evolution during conventional deformation processes, e.g. rolling, and is also expected to do the same in ECAP deformation. Many FCC metals and alloys have been studied to elucidate the effect of ECAP on microstructure and texture development, and mechanical properties, for example, Al [6–26], Ni [27–31], Cu [32–42], Au [43, 44], all with high to medium SFEs at room temperature (RT). In the case of austenitic steels [45–47] with medium-to-low SFEs at RT, ECAP has been performed at RT [45] and 300 °C [46, 47] with the SFE being in the low and medium range, respectively. Information on the evolution of microstructure and texture as a result of ECAP deformation of low SFE silver (22 mJ/m^2 [48]) is rather limited except a few papers published by the group of the present authors [49–52] in addition to a few papers by Gubicza et al. [53–55], which exclusively deal with microstructural evolution. These papers, however, present the initial results of investigation on texture evolution in ECAP deformed silver [49–52] and the role of twinning on texture evolution during ECAP, with silver as a case study [52]. Gubicza et al. [53–55] investigated the mechanisms of microstructure formation operative in silver under the conditions of SPD, primarily by X-ray line profile analysis (XLPA). However, these studies could not capture the early stages of microstructural change by virtue of the limitation of the technique. A comprehensive study was still awaited to elucidate the micro- and meso-scale aspects of ECAP deformed silver.

In the present work, an attempt has been made to understand the development of microstructure and to validate the mechanism of grain refinement and texture formation during ECAP of silver, a typical representative of low SFE materials. A thorough analysis is carried out including characterization

of microstructure as well as substructure, which together define the overall deformed microstructure. A field emission gun scanning electron microscope (FEG-SEM) with electron backscatter diffraction (EBSD) has been used for this purpose and transmission electron microscopy (TEM) for direct observations of dislocation boundaries. Textures after ECAP [56, 57] have been characterized both at global and local scale using neutron and high-energy synchrotron radiation, respectively.

Experimental procedure

Pure silver (purity 99.95%) used for the present study was received in the form of extruded bars. Prior to deformation by ECAP, the as-received material was annealed for 1 h at 350 °C in order to obtain a strain-free microstructure with equiaxed grains. Specimens with 10 mm × 10 mm square cross section and 100 mm length were machined from these annealed bars. The ECAP experiments were carried out at a cross head speed of 1 mm s^{-1} at room temperature (homologous temperature = 0.24) with MoS_2 as lubricant using a Zwick 200 kN screw driven machine and a die set with rectangular intersection of the extrusion channels (90°) without any rounding of the corner region. The number of ECAP passes was limited to 3. Between individual passes the specimen was introduced in the same sense (Route *A*, that is, no rotation around the specimen longitudinal axis between intermediate passes). No backpressure has been applied. The details of the process and the specimen for characterization are illustrated in Fig. 1.

Microstructural observations were made using a Leo scanning electron microscope operated in secondary electron (SE) mode. EBSD measurements have been carried out using a JEOL 2000 FEG-SEM with EBSD attachment. The SEM-EBSD measurements were made on ED and TD planes of the ECAP processed samples. The respective planes were metallographically polished followed by chemical polishing using a solution composed of a mixture of 10 ml saturated aqueous solution of chromium (VI) oxide and 4.5 ml hydrochloric acid (10%) in 80 ml distilled water. Special care was taken to avoid the friction affected zones of the ECAP processed samples. The EBSD analyses were carried out using the software "Channel 5" developed by HKL technology. The grain size was determined through an algorithm embedded in the software that is based on the area fraction method. A misorientation criterion of 15° was used to identify the grains. In order to identify the recrystallized grains, a grain orientation spread (GOS) value of 1.2° was used as cut-off angle.

TEM was carried out using a Philips CM20 transmission electron microscope. Thin foils for TEM were prepared by mechanical milling down to a thickness of 0.01 mm for each of the processed conditions. The samples were sectioned from the ND as well as TD

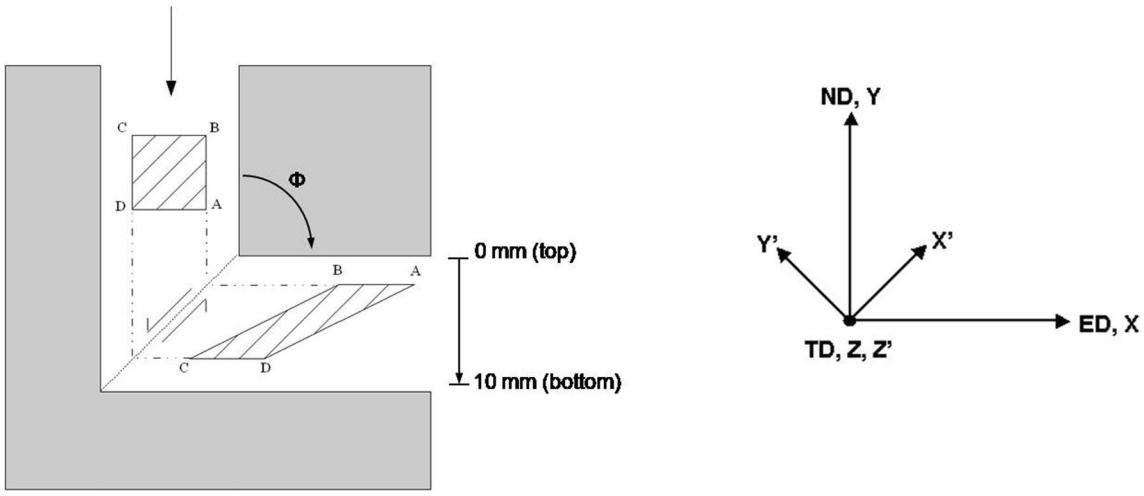

Figure 1 The simple shear model of ECAP showing the shape change of a material element with shear. (*X*, *Y*, *Z* = ECAP reference system; *X*', *Y*', *Z*' = simple shear reference system, *Y* = ND = normal direction, *Z* = *Z*' = TD = transverse direction, *X* = ED = extrusion direction) [40].

planes. Discs with 3 mm diameter were punched from the mechanically thinned foils. These discs were electro-polished using the electrolyte recommended by Bailey and Hirsch [58] for cold worked polycrystalline silver. The constituents of the electrolyte are 67.5 g potassium cyanide, 15 g Rochelle salt, 19.5 cm^3 orthophosphoric acid, 2.5 cm^3 ammonia water and 15 g potassium ferrocyanide in 1 l of the electrolyte. The voltage required across the cell was kept around 6 V. The thin foils were stored in ethanol until they were loaded in the microscope.

Bulk textures were measured by neutron diffraction at GKSS Research Centre, Geesthacht, Germany, on a cube of about 10 mm length cut from the middle of each deformed billet and also for the starting material. As the neutron texture represents the entire cube, it is therefore referred to as global texture. In order to examine the homogeneity of ECAP deformation, the local texture was analyzed by high-energy synchrotron radiation using beam line W2 (50 keV) at DESY-HASYLAB in Hamburg, Germany. The sample for local texture measurements with synchrotron radiation was a pin of 1 mm × 1 mm × 10 mm taken from the centre of the billet with the long sample axis parallel to the Y-axis. Texture was measured at 5 positions along the Y-axis. Details of the synchrotron texture measurement are given in [59].

Results

Microstructure

The microstructure of the starting material is characterized by recrystallized, almost equiaxed grains within the size range 30–40 μm displaying a few annealing twins. Substantial refinement of the microstructure occurs during ECAP, as revealed through SEM. The image quality (IQ) microstructure obtained by EBSD with superimposed grain boundaries on the cross section is presented in Fig. 2. Figure 2a, c and e shows the presence of both low angle grain boundaries (LAGBs) and high angle grain boundaries (HAGBs) of certain misorientation ranges from 5° and above coloured according to the colour bar given. Relatively large grains (20 μm) along with finer ones (< 1 μm) are apparent from Fig. 2a. Figure 2b, d and f shows the presence of twins in the microstructure, most of them being (5–8 μm) long and (1–2 μm) wide.

In order to appreciate the shear effect on the microstructure, the TD plane was also examined by EBSD. On this section (Fig. 3a, c), the "band-type" microstructure is more visible. Observation on this plane further confirms the presence of a large fraction of HAGBs as well as long and thin twins. One of the interesting observations at this stage is the coexistence of relatively large and very fine grains. The average grain size, as measured on the TD plane, after the first pass was about 1.2 μm. After 3 passes, it decreased to about 0.5 μm (Fig. 4). The steady-state grain size is almost reached. During ECAP, the grains become elongated (Fig. 3). The angle between grain long axis and extrusion direction α changes with the number of passes from 22° over 14° to 10°, in good agreement with the shape changes that take place using the flow line model of Toth et al. [32] with flow line exponents of 6, 4 and 4, which lead to the values of 22.7°, 10.7° and 4.3°, for the first, second, and third ECAP passes, respectively. However, the average aspect ratio of grains was close to 2 after the third pass, which is not in agreement with the theoretical aspect ratio of 23, also obtained from the flow line model from geometric considerations only and no grain fragmentation. This discrepancy indicates that grain fragmentation is taking place during extrusion. Further microstructural analysis has been carried out to separate recrystallized grains if any, from the deformed matrix using the GOS criteria. It was found that there was no significant volume fraction of recrystallized grains at this stage.

The finer aspects of the deformed microstructure, as revealed by TEM, vary substantially from one area to another. The occurrence of twins as revealed in EBSD micrographs could also be seen by TEM (Fig. 5c, d). The size and shape of the twins clearly indicate that they are deformation twins formed as a result of ECAP, and not inherited as fragments of the annealing twins. These twins lie along {111} planes. As seen in the EBSD maps (Fig. 2a, b), some grains are twin-free and only accommodated deformation by slip. Tangled arrays of dislocations are observed, that form diffuse cell structures. The fact that these cells are fairly loose and not well defined is the result of the low SFE of the high purity silver. In the bright-field image of Fig. 5a, elongated grains containing loose dislocations cells are visible. It is also interesting to note that one of the HAGBs is strongly curved (indicated by an arrow) and separates an area containing dislocation cells from a homogeneously distributed dislocation zone. Its shape suggests that this is a moving boundary.

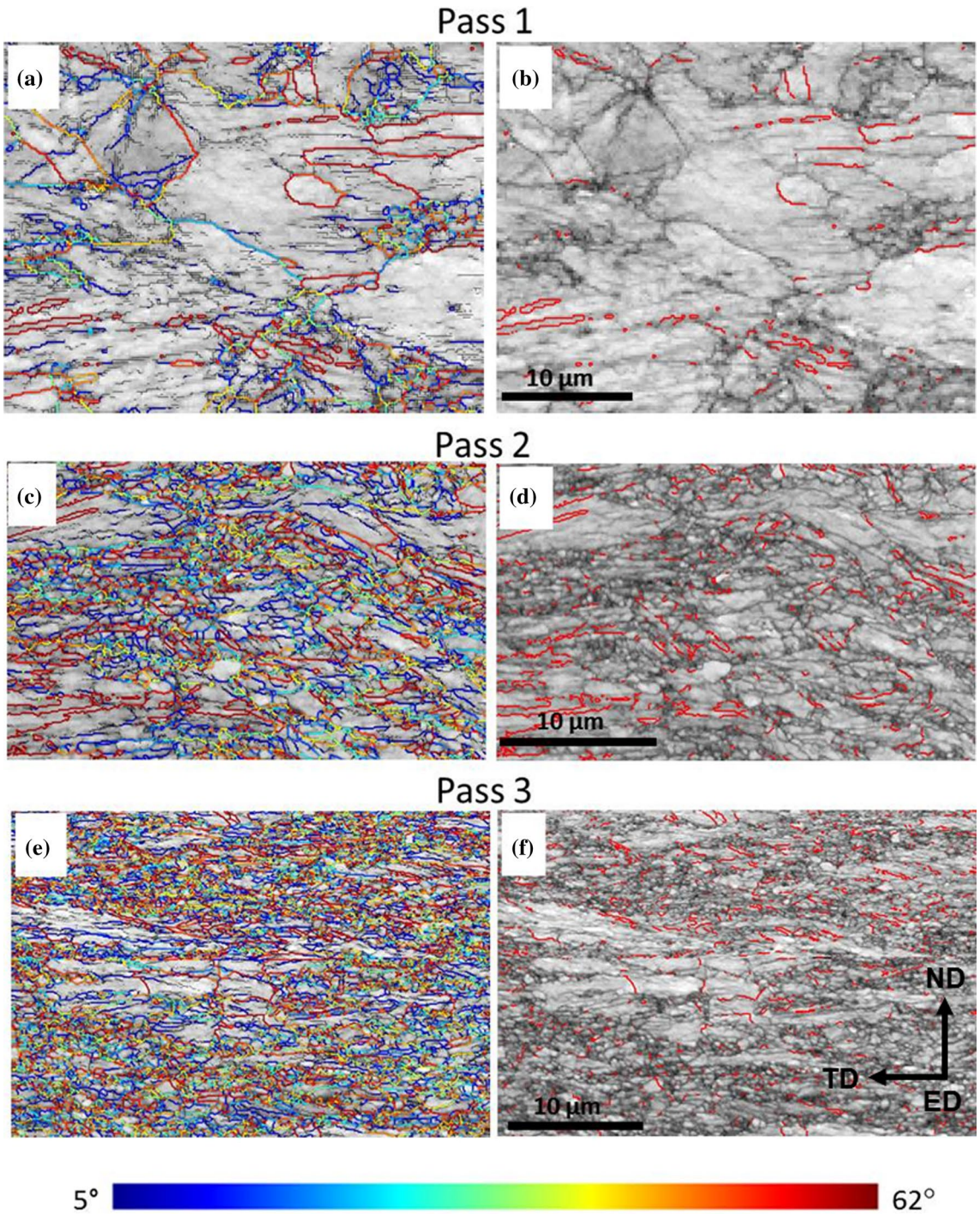

Figure 2 SEM-EBSD micrographs of the ED plane generated from the band contrast with grain boundaries imposed for samples deformed by 1, 2 and 3 ECAP passes. **a**, **c** and **e** are superimposed with the grain boundaries of certain misorientation ranges from 5° and above coloured according to the colour bar given. **b**, **d** and **f** just show the Σ3 twin boundaries (red) on the respective micrographs.

The microstructure of a sample deformed two passes as recorded by EBSD on the cross section (Figs. 2c, d) shows a decrease in the grain size with most of the grains smaller than 5 µm and a large fraction of fine grains (< 1 µm). The average grain size is about 0.6 µm. The presence of twins could also be

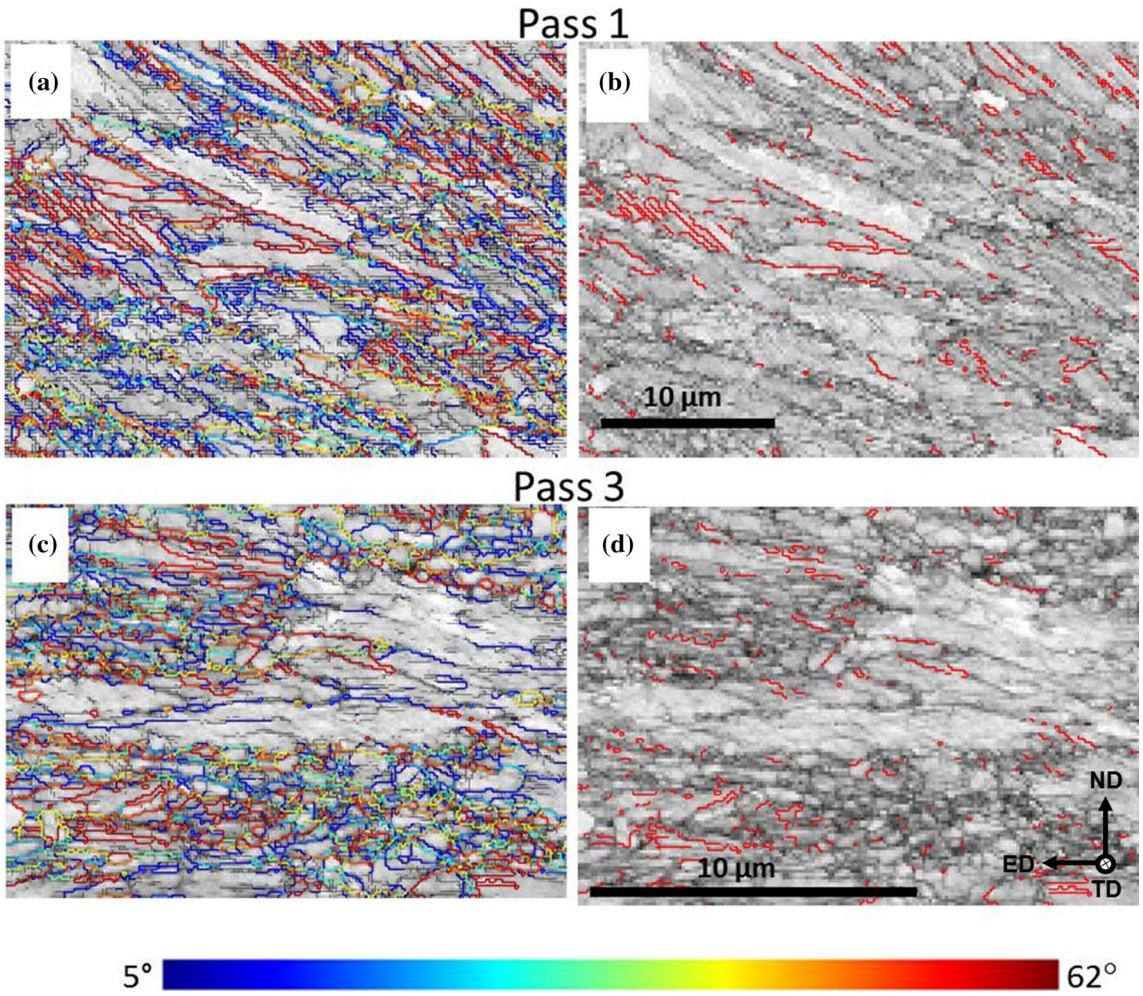

Figure 3 SEM-EBSD micrographs of the TD plane generated from the band contrast with grain boundaries imposed for samples deformed by 1 and 3 ECAP passes. **a** and **c** are superimposed with the grain boundaries of certain misorientation ranges from 5° and above coloured according to the colour bar given. **b** and **d** just show the Σ3 twin boundaries (red) on the respective micrographs.

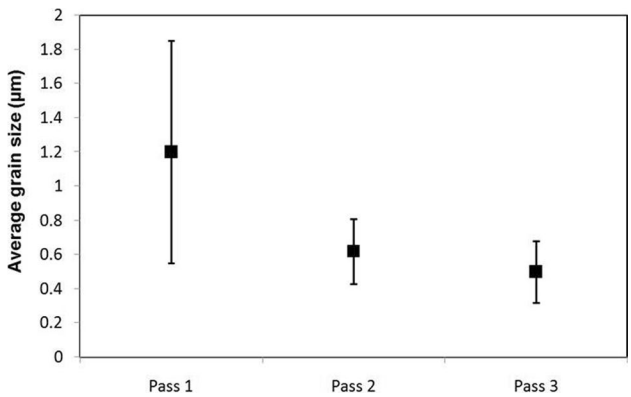

Figure 4 Grain size evolution with the number of ECAP passes.

detected. The separation of recrystallized grains following the GOS criteria results in an approximate volume fraction of about 7%.

Figure 6 shows TEM images of a banded area (Fig. 6a) with bands along {111} planes and an area containing parallel nano-twins (Fig. 6c). This micrograph illustrates that a way to reduce the apparent grain size in the ECAP processed silver is by subdivision of the initial grains by mechanical twinning (Fig. 6d).

After three passes, the microstructure recorded on the cross section (Fig. 2e, f), reveals further refinement. At this stage, many grains are refined to a size much lower than 200 nm, as confirmed by the TEM investigation. However, some larger grains are also present

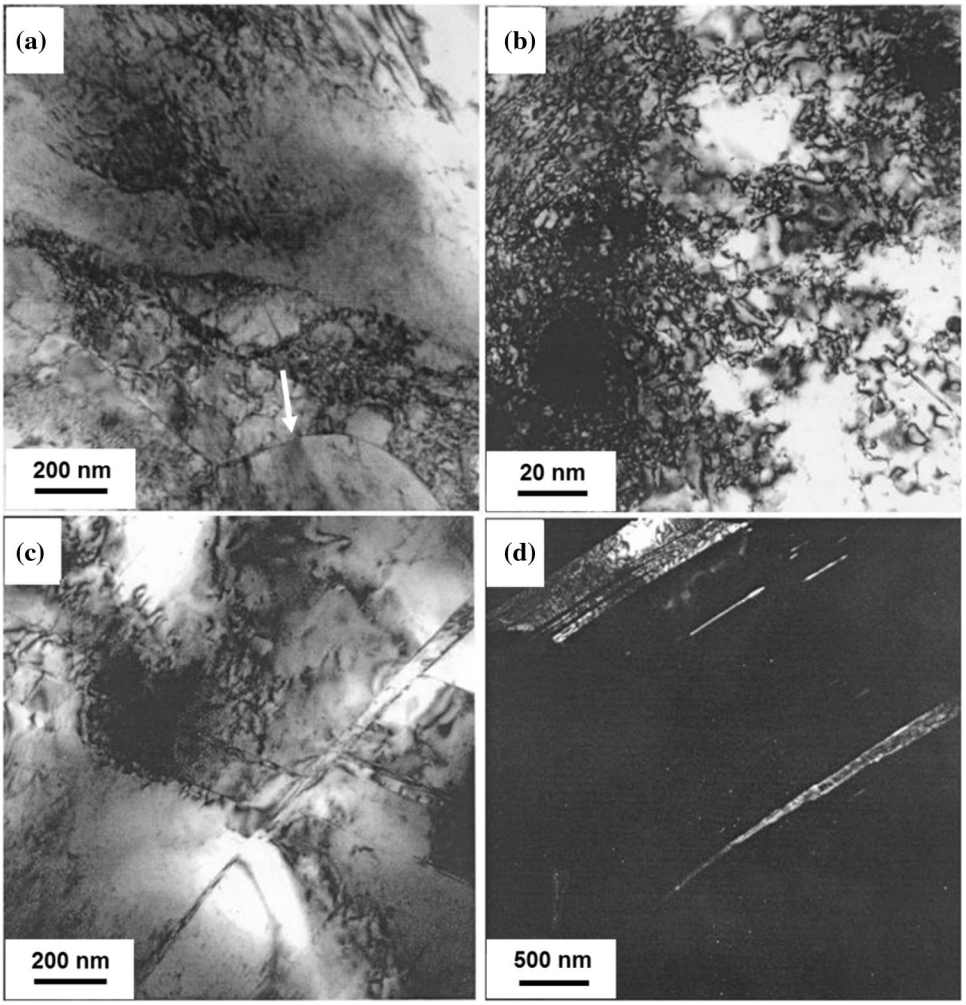

Figure 5 Microstructural features of a sample ECAP-deformed for one pass as recorded by TEM: **a** overall deformation features, **b** clusters of dislocations, **c** primary and secondary deformation twins [52], and **d** dark-field image of twins.

(~ 5 μm), which ultimately results in an average grain size of about 500 nm. Deformation bands parallel to TD are clearly visible. As seen in Fig. 3, the grains are elongated in ED and flattened in ND, a phenomenon consistent with shearing. However, the average aspect ratio of the grains after this stage is close to 2, excluding a few highly elongated grains. Mechanical twinning leads to a substantial increase in the fraction of HAGBs.

Figure 7 shows TEM micrographs for the three passes deformed material. Even in this case, the microstructure consists of twinned and non-twinned areas. Figure 7a shows a bright-field image of parallel twins containing some tangles of dislocations. After three passes, the microstructure appears more intricate and consists of a smaller fragment size. An interesting observation made quite extensively is that many grain boundaries show significant bulging illustrated in Fig. 7b. This type of bulging of the grain boundaries is a typical feature of the so-called strain-induced boundary migration (SIBM) mechanism, shown also in Fig. 5a.

Texture

Global texture

The texture of the starting material consists of a weak < 110 > fibre [51] along the billet axis entering the ECAP channel in Y direction. The bulk texture after 1, 2 and 3 passes, as measured by neutron diffraction, is shown in Fig. 8 by $\varphi_2 = 0°$ and 45° ODF sections which for FCC metals contain all major ECAP texture components. The intensity levels are chosen with respect to the ODF maxima of the corresponding samples in such a way that the orientation density is well illustrated. A key figure representing the ideal components of ECAP textures, as they appear in these sections of the ODF, is

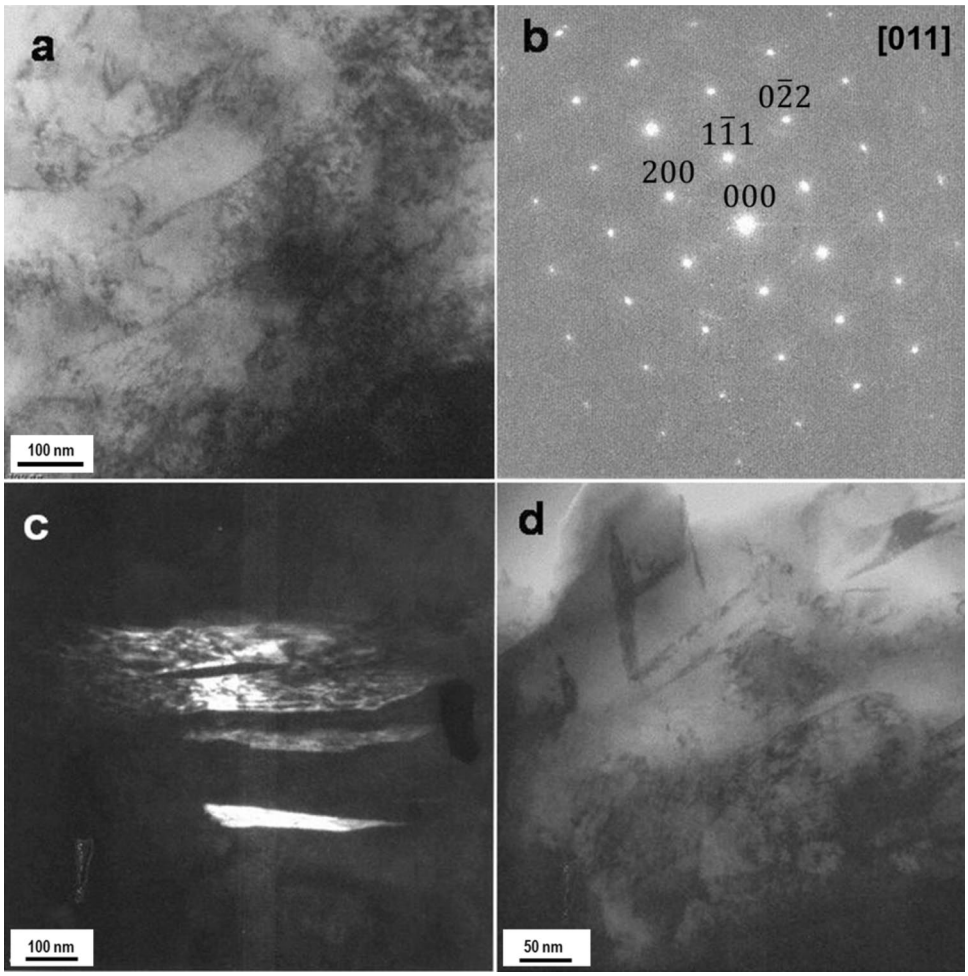

Figure 6 Microstructural features of a sample ECAP-deformed for two passes: **a** bright-field image showing parallel bands of dislocation walls, **b** diffraction pattern of grain in (**a**), **c** dark-field micrograph showing micro-twins [52], **d** primary and secondary deformation twins.

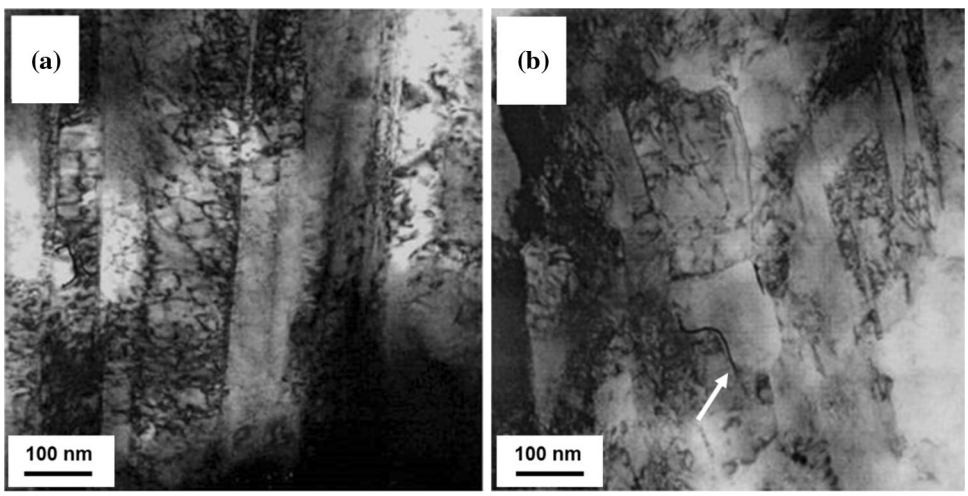

Figure 7 TEM bright-field images showing microstructural features of the three passes deformed ECAP sample: **a** parallel micro-twins [52], **b** bulging along the grain boundaries indicated by arrow revealing SIBM as a mechanism present in the material.

also given. The nomenclature of the components with regard to the shear plane and shear direction (Fig. 1) is shown in Tab. 1. The texture is clearly dominated by the $B/\overline{B}$ shear components, minor shear components are $A/\overline{A}$, A_1^*, A_2^* and C. This type of texture is characteristic of the so-called brass-type shear texture. In order

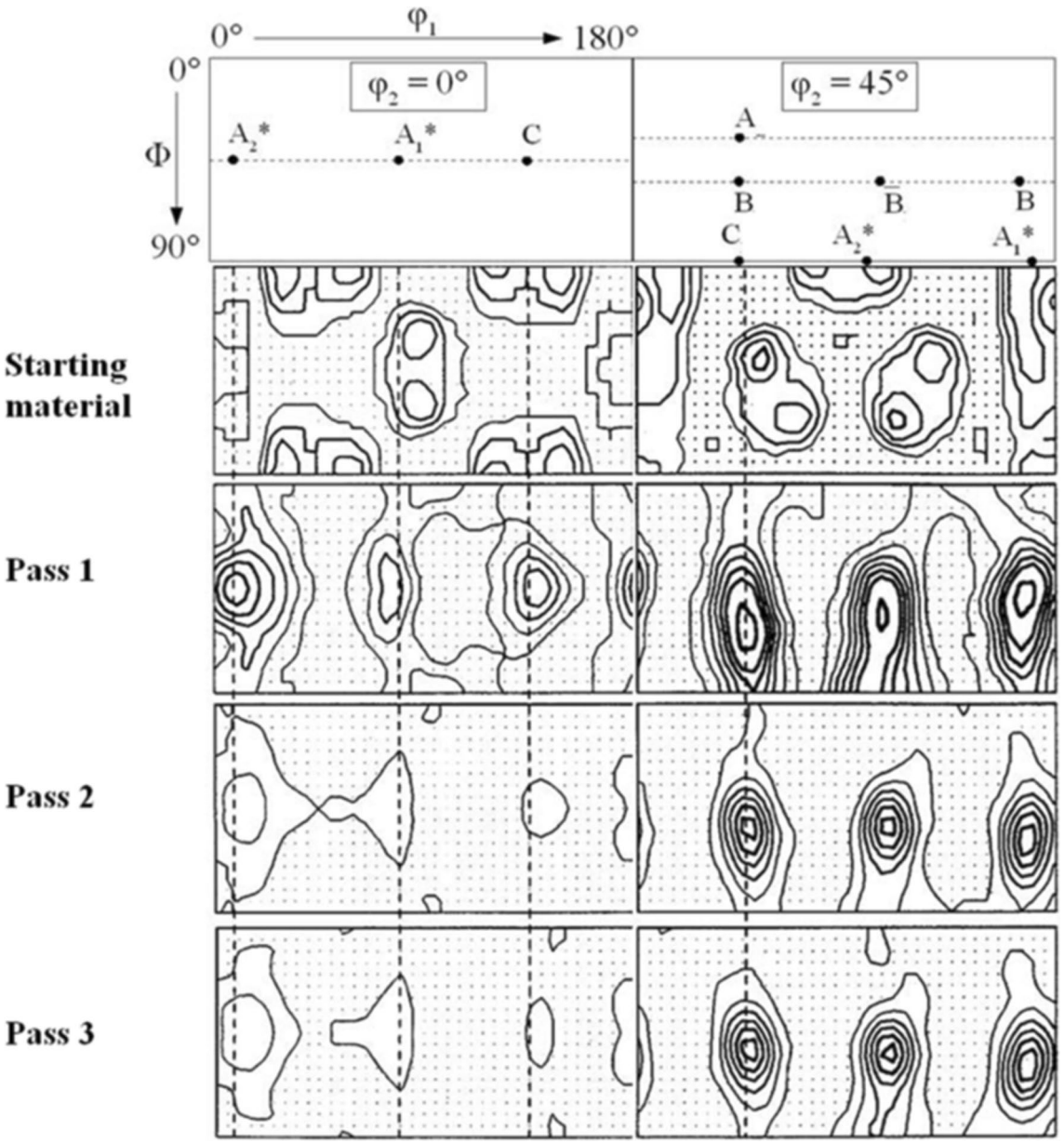

Figure 8 Experimental ODF sections as obtained by neutron diffraction for starting material, pass 1, 2 and 3. The shear components developing during ECAP in FCC metals and their positions within the $\varphi_2 = 0°$ and 45° ODF sections are given in the key figure.

to have a better visualization and quantification of the variation of texture, the ODF intensities of respective texture components and their deviation from the ideal positions have been plotted against the number of passes (Fig. 9). The intensity of the $B/\overline{B}$ component saturates after the 2nd pass, while that of the minor components decreases in the 2nd pass and seems to stay constant in further passes, too. Moreover, the components are slightly shifted in φ_1 from their ideal positions.

Local texture

Figure 10 displays the sequence of the ODF sections from the top to the bottom of the ECAP processed silver. These sections typically represent the local texture at different positions, namely at 1, 3, 5, 7 and 9 mm from the top of the ECAP bars. The disposition of texture components in the ODF sections indicates the presence of a texture gradient with respect to position. The maximum change is observed in the

Table 1 Nomenclature of shear texture components for FCC metals with regard to the shear plane and shear direction

Component designation	Miller indices {shear plane} < shear direction >
A	$\{1\bar{1}1\} < 110 >$
$\bar{A}$	$\{\bar{1}11\} < \bar{1}10 >$
A_1^*	$\{\bar{1}11\} < 112 >$
A_2^*	$\{11\bar{1}\} < 112 >$
B	$\{\bar{1}12\} < 110 >$
$\bar{B}$	$\{1\bar{1}2\} < \bar{1}10 >$
C	$\{001\} < 110 >$

lowest section. The intensity and the deviation from the respective ideal position are different for different texture components (Fig. 11).

For all the passes the $B/\bar{B}$ components are the strongest and their intensity increases with the number of passes, similar as in the global texture (Fig. 9). The texture gradient of the $B/\bar{B}$ components with respect to deviation from the ideal position in the upper sample section (0–7 mm) is about − 1.3°/mm, − 0.7°/mm and − 0.9°/mm for pass 1, 2 and 3, respectively. In the bottom part (9 mm), the intensity drastically decreases while the deviation in position increases again yielding a positive texture gradient in pass 3. There is a rough agreement of the average intensity and average deviation of $B/\bar{B}$ with that measured in the mid-plane (5 mm from top) of the billet, but this may be fortuitous. Components other than $B/\bar{B}$ are better recorded by neutrons because of a much higher volume measured, albeit globally.

Discussion

Microstructure evolution

By now, it is well established that during route A ECAP the shearing of the grains leads to an elliptical grain shape with the major axis inclined to the direction of shear (Fig. 3). This may lead to deformation banding yielding grain refinement, as different parts of the elongated grain when passing through the deformation zone along the channel intersection plane experience different strain rates. Thus, deformation bands could be either due to the ambiguity associated with the selection of the operative slip systems, as in many cases, the imposed strain can be accommodated by more than one set of slip systems leading to different lattice rotations, or by inhomogeneous straining, due to the fact that different regions of a grain may experience different strains if the work done within the bands is less than that required for homogeneous deformation and if the bands can be arranged so that the net strain matches the overall deformation. These deformation bands are separated by geometrically necessary boundaries (GNBs). An additional factor for grain refinement in Ag is twinning. Therefore, the evolution of microstructure in Ag after ECAP processing can be understood in terms of three phenomena simultaneously occurring as result of deformation,

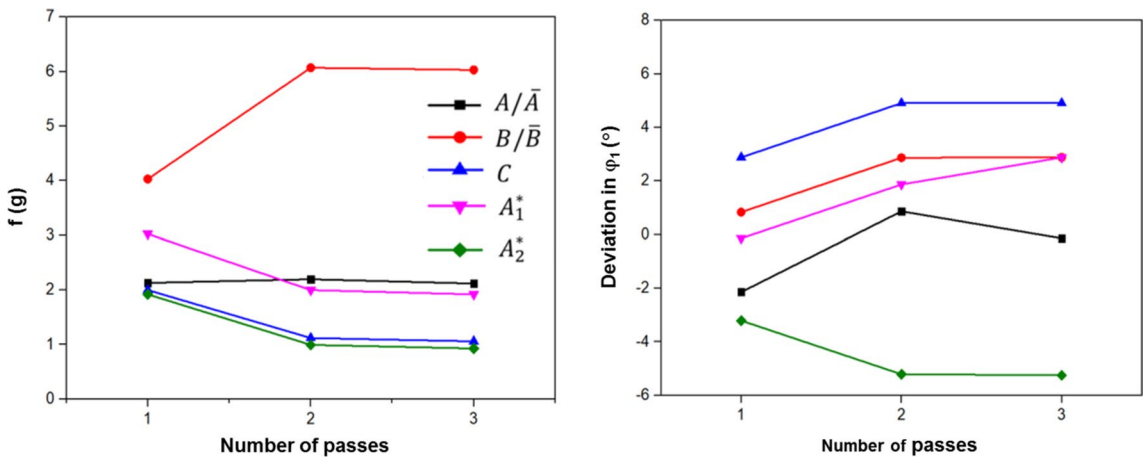

Figure 9 Intensities of texture components and deviations in φ_1 from their respective ideal positions in ECAP as a function of the number of passes.

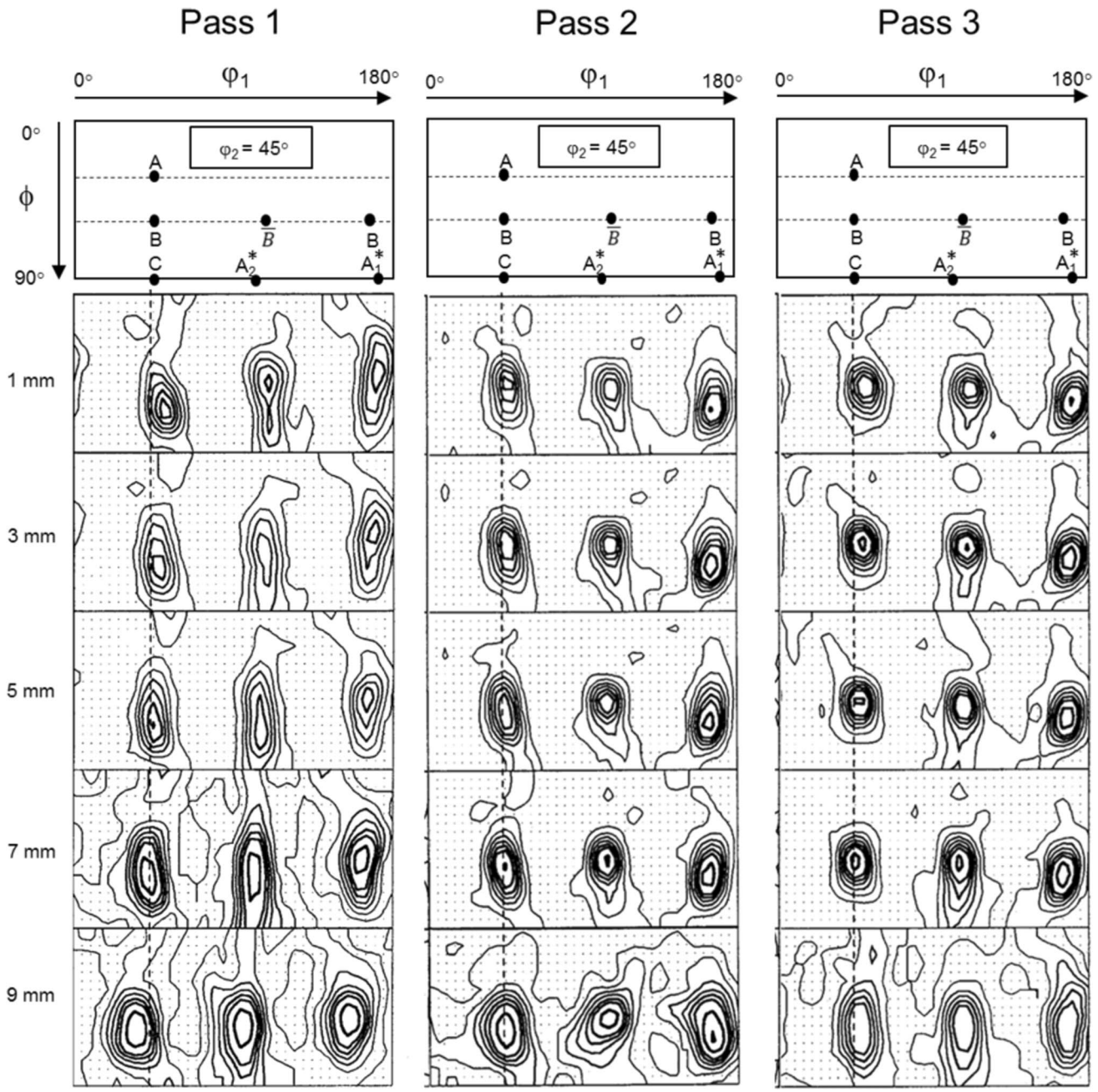

Figure 10 $\varphi_2 = 45°$ ODF sections of the textures measured using synchrotron radiation at 1, 3, 5, 7 and 9 mm from the top for pass 1, 2 and 3.

namely (1) misorientation development and overall substructure formation, (2) occurrence of twinning, and as a consequence (3) dynamic recrystallization, which could occur through SIBM. These phenomena may take place independently in different regions of the microstructure or may be correlated.

As previously mentioned, the typical cell structure in some areas of the non-twinned grains observed (Fig. 5), may not be resolved by EBSD due to limitation of this technique. In the one pass deformed silver, the tangled arrays of dislocations forming the cell structures are always fairly diffuse, so that the cells are fairly loose and not so well defined. This is consistent with the low SFE of Ag. The behaviour of the low SFE FCC metals in ECAP-type of deformation is only partially studied compared to other ECAP-deformed

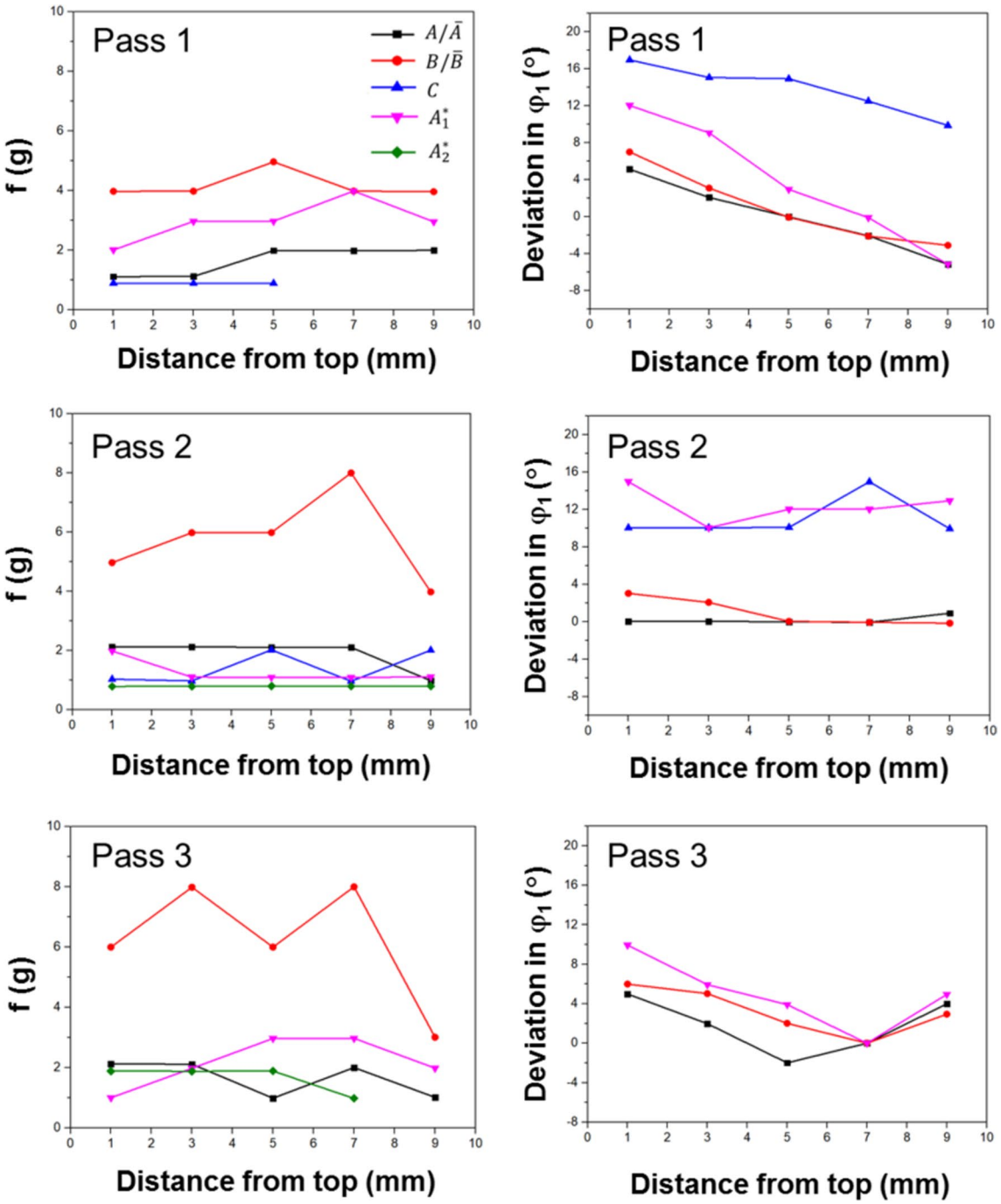

Figure 11 Orientation density and deviation in φ_1 from the ideal position of the texture components from top to the bottom of the ECAP samples.

materials. In the comprehensive study of Bailey and Hirsch [58] on the evolution of substructure in silver as a function of tensile deformation, it was reported that under a tensile deformation ≥ 30%, dislocations remain arranged in complex bands separating relatively dislocation-free areas. The cell structure becomes pronounced with increasing deformation, while at low deformation the dislocation density is more uniform. However, as the amount of deformation is quite high even after 1 pass of ECAP ($\gamma = 2$), the

microstructural features can be different. In the present study, the amount of strain in for one pass ECAP-deformed Ag is almost three times more than that of 30% rolled material; however, the distribution of dislocations throughout the microstructure is seen in large clusters. The original grain boundaries are still visible after deformation. For large deformations, studies of microstructure evolution are limited to rolled (or plane strain compression deformed) materials because of its industrial significance. Although micro-scale shear bands were reported to be a dominant feature of the microstructure at large strains in rolled low SFE FCC metals such as 70/30 brass [60], features like those are not observed in the microstructure of the ECAP deformed Ag. It is, therefore, understood that the microstructural evolution in ECAP processed Ag does not follow the trends observed in conventional deformation processes. The two major reasons for this are (1) the occurrence of twinning in silver that also occurs after 3 passes and (2) the large amount of strain imposed very locally that triggers some sort of recrystallization phenomena.

Microstructural observations clearly indicate that twinning occurs in every pass. It should be mentioned here that some annealing twins are already observed in the starting material. However, their fraction is quite low compared to the deformed materials. Moreover, due to incorporation of lattice dislocations into the twin boundaries they get converted into grains with random HAGBs. TEM observations confirm the occurrence of deformation twinning at every stage of deformation process. Each pass will generate new twins, the nucleation of which can be facilitated by remnant dislocations originating from the deformed prior twins, that is, newly activated twins can grow using twinning dislocations or defects left behind from old twins. For example, Fig. 6 shows the presence of dislocations within the twins. An increasing twin probability with increasing number of passes has also been observed by XLPA in route B_C deformed silver [54].

It is well known that continued deformation leads to increasing misorientations, which may further give rise to new HAGBs through dynamic recovery and continuous dynamic recrystallization (CDRX). In general, in low SFE materials like silver, it is expected that recovery processes will be retarded; therefore, an early initiation of recrystallization is expected. In the present case however, CDRX—in particular after 3 passes—has been found to be concomitant with SIBM. Local inhomogeneities developed in the deformed structure are the triggering feature for SIBM. Indeed, the driving force for this type of bulging event is likely to arise from a difference in dislocation density on both sides of the HAGBs. It has also been reported for deformed Al bicrystals with a twin boundary, as an effect of piled up dislocations [61]. While SIBM is a recrystallization mechanism that can be particularly important in some materials after low strains [62], it is observed here after a significant amount of strain has been imparted to the sample. Normally, SIBM results in grain coarsening rather than refinement. It is a process that contributes to the steady state grain size.

Strain-induced grain evolution during cold deformation of pure Cu by multi- directional forging was studied by Belyakov et al. [63]. The structural changes at low moderate strains in this case were attributed to the evolution of elongated subgrains with their dense dislocation boundaries, and to the strain path change promoting the formation of mutually crossing dense dislocation walls and an increase in its density with increasing deformation. This leads to the formation of a strain-induced new grain structure as a result of the gradual increase in misorientation between subgrains. This mechanism of microstructure evolution is similar to that operating during CDRX. Miura et al. [64] have reported a similar mechanism of microstructural evolution in a severely deformed 70/30 brass, where the twin boundaries are subjected to SBIM.

As SBIM is much less observed after one pass of ECAP than after three passes, it is unlikely that the difference in the rate of storage of dislocations, which depends on grain orientation, is the only driving force for bulging here. More likely, it may also arise from preferential recovery in the vicinity of grain boundaries that enables it to lower the dislocation density. From studies on Al, Cu and Fe, it appears that moderate degrees of deformation favour the coalescence of subgrains as the initiating step for forming a nucleus. On the other hand, Randle [65] reported that in low SFE materials, extensive twinning accumulates strain energy in the material, causing subsequent selective grain boundary migration. Therefore, high strain and low SFE favour SIBM in ECAP silver.

After a sufficient amount of strain has been imparted, these bulging events represent a process by which the excess amount of dislocations introduced in the material can be dissipated. After 3 passes of ECAP deformation, the material has therefore entered a stage at which the grain size tends to reach equilibrium and the grain size

reduction should become much less effective under subsequent deformation.

The need of SIBM to nucleate dynamic recrystallization here, instead of the more conventional mechanism involving nucleation of highly misoriented domains that would release more efficiently the deformation energy, has two consequences on the material behaviour:

1) The stored energy in the material remains quite high and even increases with the number of passes due to slow recovery. This is verified by DSC based studies [66].
2) Because of the formation of slightly misoriented domains, there is no texture component associated with the dynamic recrystallization process. As the new grains generated by the bulging event have very similar orientations to the grains from which they have grown, the texture modifications occurring at this stage of deformation are very limited. This could be the reason, why the texture does not change or even weakens significantly in spite of anticipated CDRX taking place in the material.

It may be suggested that, due to the low SFE of silver, nucleation might originate very small twins which then grow by the SIBM mechanism [67]. However, the present TEM investigation did not capture such a feature that could support this mechanism, which is quite likely to be missed due to the limited number of observations. Silver, a low SFE material is likely to undergo such a mechanism, and therefore, the first hand observation would exclude the possibility of dynamic recovery as the dominant mechanism of grain refinement.

It should be mentioned that Gubicza et al. [55] observed self-annealing in the form of recovery and recrystallization during storage at RT of silver (99,99% purity) deformed by ECAP route B_C with four or more passes. The degree and kinetics of self-annealing depend upon the number of passes imposed in ECAP and of course on the purity of the material. For the material deformed here up to three passes, it is assumed that self-annealing is negligible.

Texture evolution

Effect of twinning on texture evolution

The overall texture evolution during ECAP of silver has been comprehensively studied by the present authors [49, 52]. The texture of silver has been reported as {112}<110>, which consists of the $B/\overline{B}$ components [52], Table 1. These components already appear in the first pass. However, their intensities do not remain constant, but a gradual variation is noticed with further ECAP deformation. The rotation from respective ideal positions is also noticed in torsion by Hughes et al. [68], however, they are in opposite direction with respect to the ECAP textures. Such differences may be attributed to twinning. With increasing deformation (number of ECAP passes), the $A/\overline{A}$, A_1^*, A_2^* and C components further weaken and the $B/\overline{B}$ components strengthen (Fig. 9). It has been shown by simulation in [52] that twinning takes place in the A_1^*, C, $B/\overline{B}$ components but not in $A/\overline{A}$ and A_2^*. Due to the special orientation relationships, twin reorientation brings the twin from A_1^* to A_2^* and from B to $\overline{B}$, and vice versa. This mechanism is responsible for the strengthening and stabilizing of the $B/\overline{B}$ texture components. It is worth mentioning here that Chowdhury et al. [69] have reported slight changes in intensity and location of the texture components due to self-annealing. However, this effect is only relevant for a higher number of passes and may also depend on the route chosen for ECAP (B_C).

A dominant brass-type shear texture is observed in austenitic steel deformed by ECAP route B_C at 300 °C [46, 47]. The mechanical twinning that takes place at this temperature, even when the SFE increases to an intermediate value, as well as planar slip, which is inevitable in low SFE materials due to the dissociation of dislocations, appear to be responsible for the formation of this type of texture. Nevertheless, the origin of the brass-type texture is still controversial. A detailed discussion can be found in [70–72].

In a recent study, Ayoup et al. [73] presented a comparative analysis of texture evolution, deformation mechanisms, and dislocation density evolution in pure copper and Al-1100 alloy subjected to ECAP. For that purpose, a unique grain fragmentation model combining continuum dislocation dynamics with Taylor-Lin crystal plasticity was used [74, 75]. It would be interesting to see whether a similarly good agreement between simulation and experiment could be achieved for silver, with a significantly lower SFE leading to mechanical twinning and less dynamic recovery.

Texture heterogeneity

The texture evolution during route A of ECAP has been simulated by Tóth et al. [32] and Skrotzki et al.

[40] using a flow line model. In the following, the texture gradient will be discussed in light of this model. In order to interpret the differences in the textures as a function of the position from the top of ECAP bar (Fig. 1), possible differences between the flow lines have to be considered. Assuming an approximately constant thickness of the plastic zone around the intersection plane of the die, the shape of the flow lines is not the same, it depends on the Y coordinate. Flow lines nearer to the top are more rounded. It follows then from the flow line model that plastic strain increases as Y decreases. This is because the total accumulated plastic strain depends on the n-value of the flow line model. The smallest n value ($n = 2$) is expected at the top, i.e. $Y = 0$ mm, the largest ($n \rightarrow \infty$) at the bottom, i.e. $Y = 10$ mm (by disregarding the friction for a moment).

This increase, nevertheless, is quite limited, because the shear strain is 1.68 for $n = 2$ and 2 for $n \rightarrow \infty$. (This feature is also predicted by finite element method (FEM) results of the ECAP process [32]). As the total strain experienced along a flow line is large, this 25% difference should just slightly affect the relative intensities of the textures corresponding to different flow lines, in agreement with experiment (Fig. 11). There is, however, another effect, related to the shape of the flow lines, which leads to different rotations of the texture as a function of the n-value. As shown by Tóth et al. [32], the rotation decreases as n increases (this rotation is in the anticlockwise direction around TD and to the right in the $\varphi_2 = \text{const.}$ ODF sections). It is then expected from the flow line model that the texture is less rotated in φ_1 towards the bottom of the billet. This is happening in all passes (Fig. 11), but the gradient is lower in the 2nd and 3rd pass.

The differences in the shape of the flow lines induce differences in work-hardening. Although the maximum strain difference is about 25% between the top and bottom regions, it can create significant differences in the flow stress of the material when the rate of work-hardening is high. This is exactly the case for silver, which has a low SFE. However, the rate of work-hardening decreases strongly during the 2nd and 3rd pass as the material will be in stage IV work-hardening. The rate of hardening in this case is as low as for single slip hardening of a single crystal. This leads to less change of the shape of the flow lines in the 2nd and 3rd pass, and consequently, to a smaller texture gradient.

The above speculation can explain the rotations of the texture components; however, the friction was completely ignored in that analysis. In the following this parameter is discussed, too. Measurements of the shear strain distribution from deformed grids as well as FEM results show that there exists a zone in the bottom section of the billet (about 30% of its width) with less shear strain. This zone as well as the corner gap decreases with increasing friction. The experimental texture gradient is in good agreement with these findings. The increasing flow stress from the top to the bottom (see reasoning above) decreases the effect of friction as the layers near to the bottom are expected to be harder. This hardness gradient is working opposite to friction. Namely, the effect of friction is to reduce hardening because it makes less shear strain. For silver, friction increases from the 1st to the 3rd pass. This is indicated by the intensity decrease as well as the increase in deviation from the ideal position of components $B/\overline{B}$ in the bottom part (Fig. 11).

Similar results have been obtained for Cu, but here friction plays a bigger role from the first pass on [33]. Intensity changes of the texture components from top to bottom of the billets are less pronounced in the upper part of the billet, because at the shear strains applied a steady state has almost reached. The overall intensity as well as that in the central part of the billet increases with the number of passes, in contrast to Cu where a maximum occurs after two passes. A major difference to Cu is the predominance of the $B/\overline{B}$ component instead of A_1^*, in agreement with the change of simple shear textures with SFE. Therefore, with decreasing SFE the strongest component changes from C over A_1^* to $B/\overline{B}$. This change may be correlated with the increasing contribution of mechanical twinning. For a comprehensive discussion on deformation heterogeneities in ECAP the reader is referred to [76, 77].

Conclusions

A multi-scale characterization of microstructure and texture was carried out using EBSD, TEM, neutron and high-energy synchrotron radiation in order to explore the microstructural and textural features that develop during ECAP deformation of silver. From the investigation it is clear that ECAP generates various microstructural features in silver. This includes regions of uniformly distributed dislocations in the initial stage. At higher deformation dislocations also

arrange themselves in cells. Twinning and grain fragmentation were consistently observed after each pass. In the third pass, clear evidence of SIBM was detected. The global texture of silver after ECAP deformation resembles that characteristic for shear of FCC metals with low SFE. However, the texture exhibits heterogeneity from top to bottom of the billet, which decreases with the number of passes.

Acknowledgements

This manuscript was initiated at Institute of Solid State and Materials Physics, Dresden University of Technology, during the revisit of one of the authors (SS) under the revisiting program of the Alexander von Humboldt Foundation, Germany, and was completed during his stay at the same institute as Friedrich Wilhelm Bessel awardee. SS expresses his gratitude to the Alexander von Humboldt Foundation for the same. SS also acknowledges the support by the French State through the program "Investment in the future" operated by the National Research Agency (ANR) and referenced by ANR-11-LABX-0008-01 (Laboratory of Excellence on Design of Alloy Metals for low-mAss Structures "LabEx DAMAS, Université de Lorraine, Metz, France), for the invitation during which the experimental part of the work was performed. LST acknowledges the support from the National Research, Development and Innovation Office, Hungary, under the K143800 project; "New avenues of production of bulk and composite nanostructured metals; experiments, characterization, modelling". Thanks are due to Dr. Benoit Beausir (DAMAS and LEM3, Université de Lorraine) for his help in data analysis.

Author contributions

SS contributed to conceptualization, investigation, formal analysis, writing—original draft, and funding acquisition. WS contributed supervision, validation, writing—review & editing, and resources. NS, J-JF, H-GB and TG done investigation and formal analysis. LST contributed to supervision, validation, and resources.

Funding

Open Access funding enabled and organized by Projekt DEAL.

Data availability

The data supporting the findings of this study are available from the corresponding author (SS) upon reasonable request.

Declarations

Conflict of interest The authors declare that they have no known competing financial interests or personal relationships that could have appeared to influence the work reported in this paper.

Ethical approval No experiments involved human tissue.

References

[1] Segal VM (1995) Materials processing by simple shear. Mater Sci Eng A 197:157–164

[2] Valiev RZ, Korznikov AV, Mulyukov RR (1993) Structure and properties of ultrafine-grained materials produced by severe plastic deformation. Mater Sci Eng A 168:141–148

[3] Iwahashi Y, Horita Z, Nemoto M, Langdon TG (1997) An investigation of microstructural evolution during equal-channel angular pressing. Acta Mater 45:4733–4741
[4] Valiev RZ, Langdon TG (2006) Principles of equal-channel angular pressing as a processing tool for grain refinement. Prog Mater Sci 51:881–981
[5] Gholinia A, Prangnell PB, Markushev MV (2000) The effect of strain path on the development of deformation structures in severely deformed aluminium alloys processed by ECAE. Acta Mater 48:1115–1130
[6] Gholinia A, Bate P, Prangnell PB (2002) Modelling texture development during equal channel angular extrusion of aluminium. Acta Mater 50:2121–2136
[7] Bowen JR, Mishin OV, Prangnell PB, Juul Jensen D (2002) Orientation correlations in aluminium deformed by ECAE. Scr Mater 47:289–294
[8] Dupuy L, Rauch EF (2002) Deformation paths related to equal channel angular extrusion. Mater Sci Eng A 337:241–247
[9] Suwas S, Tóth LS, Fundenberger JJ, Eberhardt A (2005) Texture evolution in commercially pure Al during equal channel angular extrusion (ECAE) as a function of processing routes. Solid State Phenom 105:357–362
[10] Skrotzki W, Scheerbaum N, Oertel C-G, Brokmeier H-G, Suwas S, Tóth LS (2006) Texture formation during ECAP of aluminium alloy AA 5109. Mater Sci Forum 503–504:99–106
[11] Gubicza J, Chinh NQ, Gy K, Schiller I, Ungár T (2006) Microstructure of ultrafine-grained fcc metals produced by severe plastic deformation. Curr Appl Phys 6:194–199
[12] Skrotzki W, Scheerbaum N, Oertel C-G, Brokmeier H-G, Suwas S, Tóth LS (2007) Recrystallization of high-purity aluminium during equal channel angular pressing. Acta Mater 55:2211–2218
[13] Suwas S, Massion RA, Toth LS, Fundenberger JJ, Beausir B (2009) Evolution of texture during equal channel angular extrusion of commercially pure aluminum: experiments and simulations. Mater Sci Eng A 520:134–146
[14] Frint P, Halle T, Wagner MF-X, Hockauf M, Lampke T (2010) Scaling up the equal-channel angular pressing process: a study on a 6000 aluminium alloy. Mat-wiss u Werkstofftech 41:814–821
[15] Frint P, Hockauf M, Halle T, Strehl G, Lampke T, Wagner MF-X (2010) Microstructural features and mechanical properties after industrial scale ECAP of an Al-6060 alloy. Mater Sci Forum 667–669:1153–1158
[16] Frint P, Hockauf M, Dietrich D, Halle T, Wagner MF-X, Lampke T (2011) Influence of strain gradients on the grain refinement during industrial scale ECAP. Mat-wiss u Werkstofftech 42:680–685
[17] Venkatachalam P, Roy S, Ravisankar B, Paul VT, Vijayalakshmi M, Suwas S (2011) Texture evolution in an Al–Cu alloy during equal channel angular pressing: the effect of starting microstructure. J Mater Sci 46:6518–6527
[18] Jin H, Gallerneault M, Segal VM, Young PJ, Lloyd D (2011) Grain structure and texture in aluminium alloy AA5083 after equal angular channel extrusion, warm rolling and subsequent annealing. Mater Sci Technol 27:789–792
[19] Frint P, Hockauf M, Halle T, Wagner MF-X, Lampke T (2012) The role of backpressure during large scale equal-channel angular pressing. Mat-wiss u Werkstofftech 43:668–672
[20] Frint P, Wagner MF-X (2019) Strain partitioning by recurrent shear localization during equal-channel angular pressing of an AA6060 aluminum alloy. Acta Mater 176:306–317
[21] Kalsar R, Yadav D, Sharma A, Brokmeier H-G, May J, Höppel HW, Skrotzki W, Suwas S (2020) Effect of Mg content on microstructure, texture and strength of severely equal channel angular pressed aluminium-magnesium alloys. Mater Sci Eng A 797:140088
[22] Venkatachalam P, Roy S, Paul VT, Vijayalakshmi M, Ravisankar B, Suwas S (2012) The role of processing routes on the evolution of microstructure and texture heterogeneity during ECAP of Al–Cu alloy. Mater Sci Forum 702:113–118
[23] Venkatachalam P, Roy S, Ravisankar B, Paul VT, Vijayalakshmi M, Suwas S (2012) Effect of processing routes on evolution of texture heterogeneity in 2014 aluminium alloy deformed by equal channel angular pressing (ECAP). Mater Sci Technol 28:1445–1458
[24] Panigrahi A, Scheerbaum N, Chekhonin P, Scharnweber J, Beausir B, Hockauf M, Sankaran S, Skrotzki W (2014) Effect of back pressure on material flow and texture in ECAP of aluminium. IOP Conf Ser: Mater Sci Eng 63:012153
[25] Kliauga AM, Bolmaro RE, Ferrante M (2015) The evolution of texture in an equal channel pressed aluminum AA1050. Mater Sci Eng A 623:22–31
[26] Frint S, Hockauf M, Frint P, Wagner MF-X (2016) Scaling up Segal's principle of equal-channel angular pressing. Mater Design 97:502–511
[27] Zhilyaev AP, Kim BK, Szpunar JA, Baró MD, Langdon TG (2005) The microstructural characteristics of ultrafine-grained nickel. Mater Sci Eng A 391:377–389

[28] Neishi K, Horita Z, Langdon TG (2002) Grain refinement of pure nickel using equal-channel angular pressing. Mater Sci Eng A 325:54–58
[29] Grosdidier T, Fundenberger JJ, Goran D, Bouzy E, Suwas S, Toth LS (2004) On microstructure and texture heterogeneities in single crystals deformed by equal channel angular extrusion. Scr Mater 59:1087–1090
[30] Goran D, Fundenberger JJ, Bouzy E, Skrotzki W, Suwas S, Grodidier T, Toth LS (2011) Local texture and microstructure in cube-oriented nickel single crystal deformed by equal channel angular extrusion. Phil Mag 91:291–309
[31] Leuthold J, Reglitz G, Wegner M, Wilde G, Divinski SV (2016) Local texture-microstructure correlation due to deformation localization in ECAP-processed nickel. Mater Sci Eng A 669:196–204
[32] Tóth LS, Massion RA, Germain L, Baik SC, Suwas S (2004) Analysis of texture evolution in equal channel angular extrusion of copper using a new flow field. Acta Mater 52:1885–1898
[33] Li S, Beyerlein IJ, Necker CT, Alexander DJ, Bourke M (2004) Heterogeneity of deformation texture in equal channel angular extrusion of copper. Acta Mater 52:4859–4875
[34] Skrotzki W, Scheerbaum N, Oertel CG, Brokmeier H-G, Suwas S, Tóth LS (2005) Texture gradient in ECAP copper measured by synchrotron radiation. Solid State Phenom 105:327–332
[35] Li S, Beyerlein IJ, Alexander DJ, Vogel S (2005) Texture evolution during multi-pass equal channel angular extrusion of copper: neutron diffraction characterization and polycrystal modeling. Acta Mater 53:2111–2125
[36] Gazder AA, Li S, Dalla Torre FH, Beyerlein IJ, Gu CF, Davies CHJ, Pereloma EV (2006) Progressive texture evolution during equal channel angular extrusion. Mater Sci Eng A 437:259–267
[37] Li S, Beyerlein IJ, Alexander DJ (2006) Characterization of deformation textures in pure copper processed by equal channel angular extrusion via route A. Mater Sci Eng A 431:339–345
[38] Li S, Beyerlein IJ, Necker CT (2006) On the development of microstructure and texture heterogeneity in ECAE via route C. Acta Mater 54:1397–1408
[39] Suwas S, Arruffat-Massion R, Toth LS, Eberhardt A, Fundenberger JJ, Skrotzki W (2006) Evolution of crystallographic texture during equal channel angular extrusion of copper: the role of material variables. Met Mater Trans A 37:739–753
[40] Skrotzki W, Scheerbaum N, Oertel C-G, Arruffat-Massion R, Suwas S, Tóth LS (2007) Microstructure and texture gradient in copper deformed by equal channel angular pressing. Acta Mater 55:2013–2024
[41] Dalla Torre FH, Gazder AA, Gu CF, Davies CHJ, Pereloma EV (2007) Grain size, misorientation, and texture evolution of copper processed by equal channel angular extrusion and the validity of the Hall-Petch relationship. Met Mater Trans A 38:1080–1095
[42] Skrotzki W, Tränkner C, Chulist R, Beausir B, Suwas S, Tóth LS (2010) Texture heterogeneity in ECAP deformed copper. Solid State Phenom 160:47–54
[43] Suzuki T, Vinogradov A, Hashimoto S (2004) Strength enhancement and deformation behaviour of gold after equal-channel angular pressing. Mater Trans 45:2200–2208
[44] Gubicza J, Chinh NQ, Szommer P, Vinogradov A, Langdon TG (2007) Microstructural characteristics of pure gold processed by equal-channel angular pressing. Scr Mater 56:947–950
[45] Toofaninejad M, Ahmadabadi MN (2013) Effect of equal channel angular pressing on the microstructure and mechanical properties of AISI, type 304 austenitic stainless steel. Adv Mater Res 829:86–90
[46] Haase C, Kremer O, Hu W, Ingendahl T, Lapovok R, Molodov DA (2016) Equal-channel angular pressing and annealing of a twinning-induced plasticity steel: microstructure, texture, and mechanical properties. Acta Mater 107:239–253
[47] Wang L, Benito JA, Calvo J, Cabrera JM (2017) Equal channel angular pressing of a TWIP steel: microstructure and mechanical response. J Mater Sci 52:6291–6309
[48] Murr LE (1975) Interfacial phenomena in metals and alloys. Addison-Wesley, p 131
[49] Suwas S, Toth LS, Fundenberger J-J, Eberhardt A, Skrotzki W (2003) Evolution of crystallographic texture during equal channel angular extrusion of silver. Scr Mater 49:1203–1208
[50] Suwas S, Toth LS, Fundenberger JJ, Grosdidier T, Skrotzki W (2005) Texture evolution in FCC metals during equal channel angular extrusion (ECAE) as a function of stacking fault energy. Solid State Phenom 105:345–350
[51] Skrotzki W, Scheerbaum N, Oertel CG, Brokmeier HG, Suwas S, Tóth LS (2005) Texture gradient in ECAP silver measured by synchrotron radiation. Mater Sci Forum 495:821–826
[52] Beyerlein IJ, Tóth LS, Tome CN, Suwas S (2007) Role of twinning on texture evolution of silver during equal channel angular extrusion. Phil Mag 87:885–906
[53] Gubicza J, Chinh NQ, Lábár JL, Hegedűs Z, Xu C, Langdon TG (2008) Microstructure and yield strength of severely deformed silver. Scr Mater 58:775–778
[54] Gubicza J, Chinh NQ, Lábár JL, Hegedűs Z, Langdon TG (2009) Twinning and dislocation activity in silver

processed by severe plastic deformation. J Mater Sci 44:1656–1660
[55] Gubicza J, Chinh NQ, Lábár JL, Hegedűs Z, Langdon TG (2010) Principles of self-annealing in silver processed by equal-channel angular pressing: the significance of a very low stacking fault energy. Mater Sci Eng A 527:752–760
[56] Beyerlein IJ, Tóth LS (2009) Texture evolution in equal-channel angular extrusion. Prog Mater Sci 54:427–510
[57] Suwas S, Mondal S (2019) Texture evolution in severe plastic deformation processes. Mater Trans 60:1457–1471
[58] Bailey JE, Hirsch PB (1960) The dislocation distribution, flow stress, and stored energy in cold-worked polycrystalline silver. Phil Mag 5:485–497
[59] Skrotzki W, Klöden B, Tamm R, Oertel C-G, Garbe U, Rybacki E (2003) Torsion texture measurements with high-energy synchrotron radiation. Textures Microstruct 35:163–173
[60] Huber J, Hatherly M (1979) Nucleation of recrystallized grains in heavily cold-worked α-brass. Met Sci 13:665–669
[61] Kashihara K, Inoko F (2001) Effect of piled-up dislocations on strain induced boundary migration (SIBM) in deformed aluminum bicrystals with originally Σ3 twin boundary. Acta Mater 49:3051–3061
[62] Beck PA, Sperry PR (1959) Strain induced grain boundary migration in high purity aluminium. J Appl Phys 21:150–152
[63] Belyakov A, Sakai T, Miura H, Tsuzaki K (2001) Grain refinement in copper under large strain deformation. Phil Mag A 81:2629–2643
[64] Miura H, Nakao Y, Sakai T (2007) Enhanced grain refinement by mechanical twinning in a bulk Cu-30 mass % Zn during multi-directional forging. Mater Trans 48:2539–2541
[65] Randle V (1999) Mechanism of twinning-induced grain boundary engineering in low stacking-fault energy materials. Acta Mater 47:4187–4196
[66] Suwas S, Eberhardt A, Toth LS, Fundenberger JJ, Grosdidier T (2004) A recrystallisation based investigation for efficiency of processing routes during equal channel angular extrusion. Mater Sci Forum 467:1325–1332
[67] Bailey JE (1960) Electron microscope observations on the annealing processes occurring in cold-worked silver. Phil Mag 5:833–842
[68] Hughes DA, Lebensohn RA, Wenk HR, Kumar A (2000) Stacking fault energy and microstructure effects on torsion texture evolution. Proc R Soc Lond A 456:921–953
[69] Chowdhury SG, Gubicza J, Mahato B, Chinh NQ, Hegedűs Z, Langdon TG (2011) Texture evolution during room temperature ageing of silver processed by equal-channel angular pressing. Scr Mater 64:1007–1010
[70] Leffers T, Ray RK (2009) The brass-type texture and its deviation from the copper-type texture. Prog Mater Sci 54:351–396
[71] Skrotzki W, Eschke A, Jóni B, Ungár T, Tóth LS, Ivanisenko Yu, Kurmanaeva L (2013) New experimental insight into the mechanisms of nanoplasticity. Acta Mater 61:7271–7284
[72] Sathiaraj GD, Pukenas A, Skrotzki W (2020) Texture formation in face-centered cubic high-entropy alloys. J Alloys Compd 826:154183
[73] Ayoub G, Modad OAA, AaH K, Shehadeh M, Mastorakos I (2023) Strain hardening and microstructure evolution in ECAP-processed ultrafine-grained metals: a comparative study of copper, aluminum, and magnesium alloys. J Mater Sci. https://doi.org/10.1007/s10853-023-08942-1
[74] Kobaissy AH, Ayoub G, Tóth LS, Mustapha S, Shehadeh M (2019) Continuum dislocation dynamics-based grain fragmentation modelling. Int J Plast 114:252–271
[75] Zouhal N, Molinari A, Tóth LS (1996) Elastic-plastic effects during cyclic loading as predicted by the Taylor-Lin model of polycrystal elasto-plasticity. Int J Plast 12:343–360
[76] Skrotzki W (2019) Deformation heterogeneities in equal channel angular pressing. Mater Trans 60:1331–1343
[77] Edalati K, Bachmaier A, Beloshenko VA, Beygelzimer Y, Blank VD, Botta WJ, Bryła K, Čížek J, Divinski S, Enikeev NA, Estrin Y, Faraji G, Figueiredo RB, Fuji M, Furuta T, Grosdidier T, Gubicza J, Hohenwarter A, Horita Z, Huot J, Ikoma Y, Janeček M, Kawasaki M, Král P, Kuramoto S, Langdon TG, Leiva DR, Levitas VI, Mazilkin A, Mito M, Miyamoto H, Nishizaki T, Pippan R, Popov VV, Popova EN, Purcek G, Renk O, Révész A, Sauvage X, Sklenicka V, Skrotzki W, Straumal BB, Suwas S, Tòth LS, Tsuji N, Valiev RZ, Wilde G, Zehetbauer MJ, Zhu X (2022) Nanomaterials by severe plastic deformation: review of historical developments and recent advances. Mater Res Lett 10:163–256